TWO- AND THREE-DIMENSIONAL TURBINE BLADE ROW FLOW FIELD SIMULATIONS*

R.C. Buggeln, W.R. Briley, H. McDonald
S.J. Shamroth, and B.C. Weinberg
Scientific Research Associates, Inc.
Glastonbury, Connecticut

A major problem area associated with the successful design and operation of modern gas turbine engines is the turbine. This section represents a considerable challenge to both the design and research engineer as it contains significant regions of complex three-dimensional flows which include both aerodynamic and heat transfer phenomena. As a result, the turbine section has been the object of extensive investigation via both analysis and experiment. The present paper discusses work performed to date by Scientific Research Associates under the NASA HOST program in the numerical simulation of turbine passage flows via a Navier-Stokes appproach. The paper is a summation of the work performed between 1984 and 1987. This work includes both laminar and turbulent simulations in both two and three dimensions. An outline of the approach and background as well as an overview of the results follow.

APPROACH AND BACKGROUND

The present approach solves the ensemble-averaged Navier-Stokes equations via the Linearized Block Implicit (LBI) technique of Briley and McDonald (Ref. 1). Boundary conditions for subsonic inflow and outflow (the usual case) set upstream stagnation pressure, upstream stagnation temperature, upstream flow angle and downstream static pressure. Additional conditions used are density derivative on the inflow (upstream boundary), and velocity and temperature second derivatives on the downstream boundary. On the cascade blade, no-slip conditions and a zero normal pressure gradient condition are applied along with either a specified temperature or a specified heat transfer rate. In general, the first grid point off the wall is taken so as to place a point in the viscous sublayer. The governing equations are written in general tensor form and solved in a body-fitted coordinate system. The procedure can be used either for laminar or turbulent flow. When used for turbulent flow either a mixing length model or a two-equation, $k-\varepsilon$, model is available. Transition can be modeled either through the $k-\varepsilon$ equation or via a specified transition location. Details of the governing equations, numerical techniques, grid construction, turbulence model, etc. are given in References 2-4.

*The work presented here has been performed under NASA Contract NAS3-24358 and NAS3-23695. Work under the latter contract was performed under subcontract to Allison Gas Turbine Operations.

INITIAL C3X - "O"-GRID RESULTS STUDIES

The computational efforts pursued under this program all considered the Allison C3X turbine cascade configuration. A computer generated plot of this configuration with an O-type computational grid is shown in Figure 1. This coordinate system consists of 30 points in the pseudo-radial direction and 120 points in the pseudo-azimuthal direction. The upstream boundary is placed at 2.25 axial chords upstream of the leading edge and the downstream boundary is placed at 2.65 axial chords downstream of the trailing edge. High radial resolution is obtained near the surface of the blade, with the first coordinate line located at a distance of 1.0×10^{-6} axial chords from the surface which is within the turbulent boundary layer viscous sublayer. In addition, high pseudo-azimuthal resolution is obtained at both leading and trailing edges.

Calculations made with the SRA procedure using this grid are shown in Figure 2. The case was run with flow parameters corresponding to test case 144 of Reference 5. The parameters were a ratio of upstream total to downstream static pressure of 1.66, an exit Mach number of 0.90, an exit Reynolds number of 2.43×10^{6}, a ratio of average blade surface temperature to inlet gas total temperature of 0.75 and an average inlet turbulence intensity of .065. Figure 2 shows a comparison between data, the present Navier-Stokes approach and the inviscid approach of Delaney (Ref. 6). There is excellent agreement between the present calculations and the experimental data. Mixing length and k-ε two-equation turbulence models were employed, and (as expected) the result of calculations indicate very little difference in the prediction of the pressure coefficient. Due to the small viscous displacement effect, the inviscid calculations show close agreement with the present computed results. Also shown in this figure are the data from cases 148 and 158, which were run under nominally identical conditions (cf. Ref. 5) to indicate the relationship between the calculations and the experimental scatter.

In Figure 3 the distribution of the computed heat transfer coefficient is shown for case 144 with both film-cooling and non-film-cooling options. For the non-film cooling option, with the local surface temperature distribution given in Reference 5, a mixing length turbulence model in conjunction with a transition model was employed for which laminar flow was assumed in the region $x/c_x < 0.2$ followed by a transitional zone and thereafter by fully turbulent flow. The predictions obtained with the model compare very well with the experimental data taken with no film-cooling present. Following this initial calculation, the film-cooling option in the code was activated with air injected at 30° to the suction side over $0.8 < x/c_x < 0.9$ at a velocity of 7% of freestream. The local surface temperature was kept fixed at the same value as the non-film-cooling option. Although no data is available for comparison, the calculation does demonstrate the effect of film-cooling. From the onset of injection to the trailing edge the heat transfer rate drops to nearly zero. This behavior is a consequence of the buffer region of constant temperature cool gas which protects the blade surface from the hotter fluid in the cascade passage. The comparison of the pressure distribution for both film cooling and non-film-cooling options is shown in Figure 4. The effect of blowing on the pressure distribution is clear; i.e. the adverse pressure gradient that is generated, the resulting upstream influence, and the subsequent favorable pressure gradient that follows.

Following the two-dimensional calculations, a demonstration three-dimensional calculation was performed. A rectilinear cascade with the C3X geometry was assumed and a grid consisting of 100×25×15 points was used. For this demonstration case laminar conditions were assumed. The height of the blade above the endwall (to the symmetry plane, midspan) was set to be one axial chord, while the inlet boundary layer thickness was 20% of that value. In Figure 5, the velocity vector plots are presented for the forward portion of the C3X cascade at two different planes above the endwall. Very near the endwall (within 2.95% spanwise plane) a saddle point exists as indicated in the picture. This saddle point moves toward the leading edge and disappears beyond 2.95% spanwise plane. A stagnation point forms on the nose of the blade surface beyond 2.95% spanwise plane.

CONVERGENCE STUDIES

An important aspect of a practical Navier-Stokes calculation procedure for flows in which a steady solution is sought is that of rate of convergence to steady state. Rate of convergence to steady state and run time per time step or iteration determine run time to convergence. This run time determines the practicality of the procedure for use on a regular basis. Therefore, under the HOST effort a study of the existing convergence rate of the SRA procedure was undertaken.

The initial test case chosen for the convergence study was the Turner turbine cascade (Ref. 7). The convergence study calculation was run with a 'C' grid containing 113 pseudo-azimuthal grid points and 30 pseudo-radial grid points. High wall resolution was obtained with the first point off the wall being approximately 1.5×10^{-5} chords from the blade surface. In regard to convergence, several criteria can be considered. These include surface pressure distribution, maximum normalized residual and pressure coefficient at the stagnation point. In regard to these factors, it should be noted that in the present calculations it is the converged steady state flow field which is the item of interest. Therefore, although the current numerical procedure solves the unsteady flow equation, it is not necessary and, in fact, is uneconomical to obtain a time-accurate solution when seeking steady state solutions. Instead, matrix preconditioning techniques are used to obtain a converged solution as rapidly as possible. In these studies, the calculation was initiated from a very simple flow field in which the velocity magnitude and static pressure were set to constant throughout the flow with the velocity flow angle a function of axial location. Very simple profiles were used near the blade surface to bring the velocity to the no-slip condition.

A plot showing the maximum normalized flow residual is presented in Figure 6. The residual is defined as the imbalance of all steady terms and is normalized by the residual at the first time step. As can be seen, the maximum residual drops slightly over 4 orders of magnitude in 150 time step iterations and then levels. In general, based upon previous experience, three orders of magnitude drop in residual gives convergence suitable for many engineering applications. However, in addition to monitoring the residual behavior it is necessary to consider the flow field dependent variable behavior. Based upon experience, one sensitive item is the pressure coefficient at the stagnation point where C_p is taken as $(p-p_{ref})/\frac{1}{2}\rho_{ref}q^2_{ref}$.

The reference quantities are taken from the inflow boundary and consequently, since only total pressure, total temperature and flow angle are specified, these may vary with time. The results show the variation of stagnation point C_p with time-step iteration number. The calculation was run with an inflow Mach number of approximately 0.24; on an inviscid basis this should lead to a stagnation point C_p of 1.015. The present results converge to a value of approximately 1.005 for the Navier-Stokes simulation. As can be seen in Figures 7 and 8, the stagnation point C_p was obstensibly converged at 100 time steps although some slight oscillations occurred until 150 time steps.

The next set of convergence studies focused upon the C3X grid. Again a C-grid configuration was used. Convergence history results for a two-dimensional laminar calculation are given in Figure 9. As can be seen, the residual drops five orders of magnitude in 150 time steps. It is also of interest to note that doubling the number of grid points did not significantly effect the convergence rate. The convergence rate for the three-dimensional case is shown in Figure 10. Again, rapid convergence is obtained. A study of the two-dimensional turbulent C3X case is shown in Figure 11. The results shown in Figures 6-11 clearly indicate the rapid convergence attainable with the present procedure and its potential for use as an engineering tool.

FURTHER C3X CALCULATIONS

The last set of calculations performed to date consist of laminar and turbulent simulations for both two- and three-dimensional C3X configurations. Calculations were performed on a C-type computational grid. Both mixing length and two-equation turbulence models were utilized. Mach number contours are shown in Figure 12 for laminar and turbulent flow. The main difference in these cases is that the shear layers are very thin in the turbulence case and much thicker in the laminar case. Other typical results are shown in Figures 13 and 14 which show results for two-dimensional simulations using a two-equation $k-\varepsilon$ model. Calculations were also performed for three-dimensional simulations. Typical grids in a given plane parallel to the endwall are shown in Figure 15. Figure 16 presents velocity vectors in a plane adjacent to the endwall; the appearance of the saddle points is clearly evident. Velocity vector plots for surfaces normal to the endwall are shown in Figure 17.

SUMMARY AND CONCLUSIONS

Under the HOST effort, SRA has further developed and applied a cascade Navier-Stokes analysis to the turbine blade row problem. Calculations have been performed in two and three dimensions for both laminar and turbulent flow. Comparisons made with data for surface pressure and surface heat transfer distribution showed good agreement. The computed three-dimensional flows showed the physically expected flow features. Calculations required relatively short run times to convergence. Two-dimensional calculations for 3500 grid points required approximately 60 CPU secs of CRAY-XMP time whereas three-dimensional calculations for 170,000 grid points required approximately 2.5 hours of CRAY CPU time. Clearly, the two-dimensional analysis can be used on a regular engineering basis. Although run times for the three-dimensional calculation preclude daily use, they are still short enough to allow the three-dimensional analysis to be used as a design tool in conjunction with two-dimensional analyses, more approximate three-dimensional analyses and experiments.

REFERENCES

1. Briley, W.R. and McDonald, H.: Solution of the Multidimensional Compressible Navier-Stokes Equations by a Generalized Implicit Method. Journal of Computational Physics, Vol. 24, 1977, p. 372-397.

2. Shamroth, S.J., McDonald, H. and Briley, W.R.: Prediction of Cascade Flow Fields Using the Averaged Navier-Stokes Equations. ASME Journal of Engineering Gas Turbines and Power, Vol. 196, 1984, pp. 383-390.

3. Yang, R.-J., Weinberg, B.C., Shamroth, S.J. and McDonald, H.: Numerical Solutions of the Navier-Stokes Equations for Two- and Three-Dimensional Turbine Cascades with Heat Transfer. SRA Report R85-310004-F, 1985.

4. Weinberg, B.C., Yang, R.-J., McDonald, H. and Shamroth, S.J.: Calculations of Two- and Three-Dimensional Transonic Cascade Flow Fields Using the Navier-Stokes Equations. ASME Paper 85-GT-66, 1985.

5. Hylton, L.D., Mihelc, M.S., Turner, E.R., Nealy, D.A. and York, R.E.: Analytical and Experimental Evaluation of the Heat Transfer Distribution Over the Surface of Turbine Vanes. NASA-CR-168015, May 1983.

6. Delaney, R.A.: Time Marching Analysis of Steady Transonic Flow in Turbomachinery Cascades Using the Hopscotch Method. ASME Journal of Engineering for Power, Vol. 105, 1983, pp. 272-279.

7. Turner, A.B.: Local Heat Transfer Measurements on a Gas Turbine Blade. Journal of Mechanical Engineering Sciences, Vol. 13, 1971.

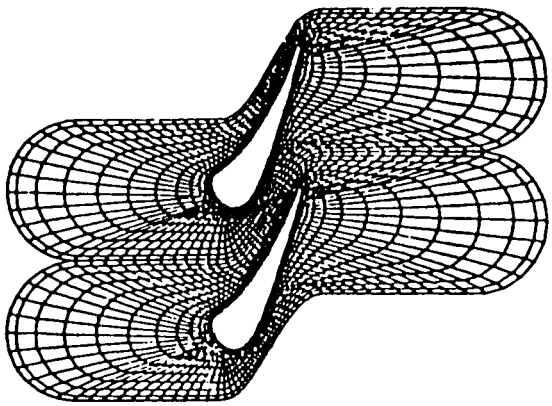

Fig. 1 C3X Turbine Blade "O"-Grid Mesh.

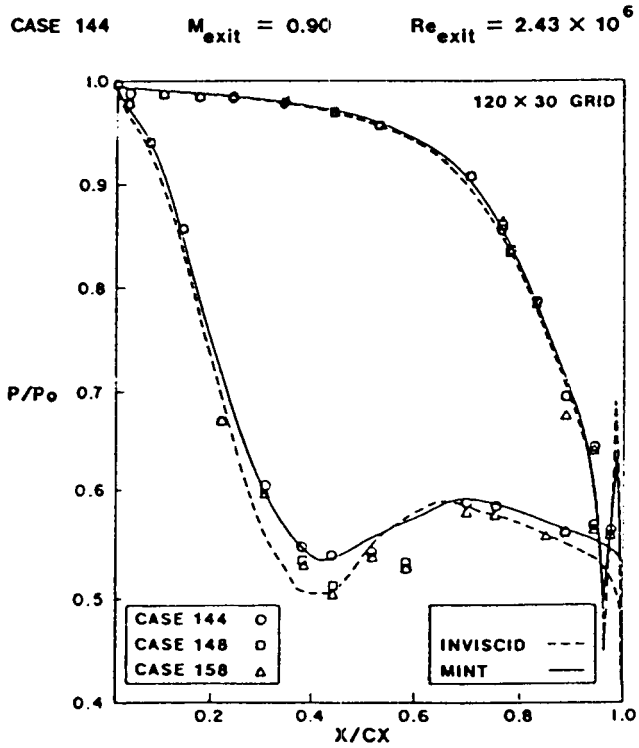

Fig. 2 Pressure Coefficient Distribution.

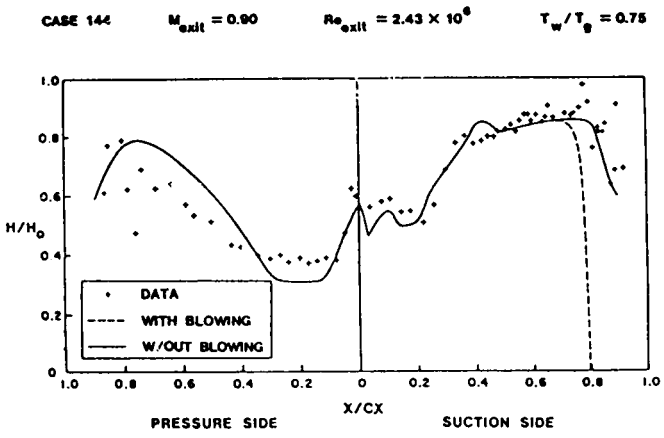

Fig. 3 Heat Transfer Coefficient.

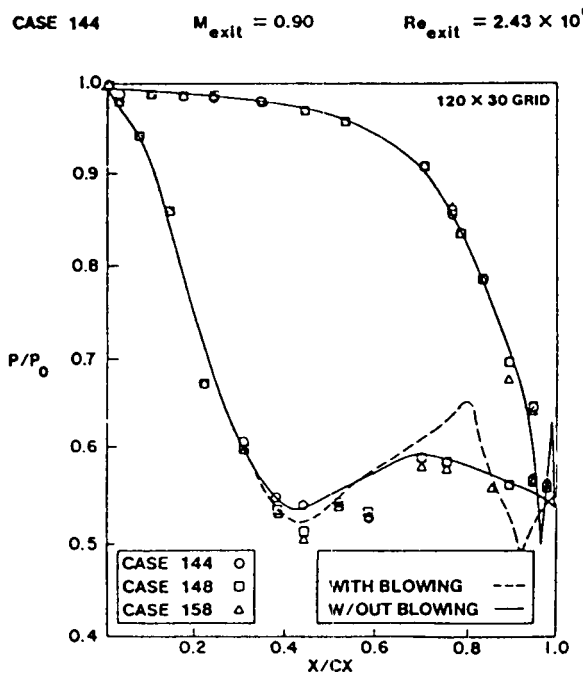

Fig. 4 Pressure Coefficient Distribution.

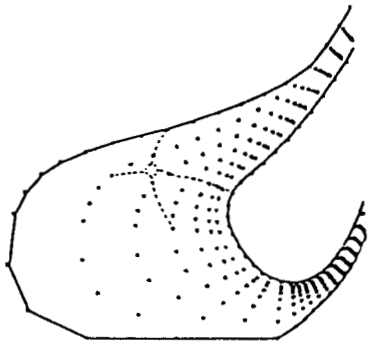

(a) VECTOR PLOT ON 0.135% SPANWISE PLANE

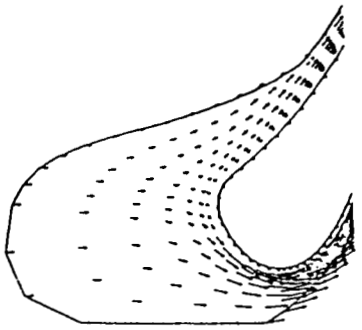

(b) VECTOR PLOT ON MIDSPAN PLANE

Fig. 5

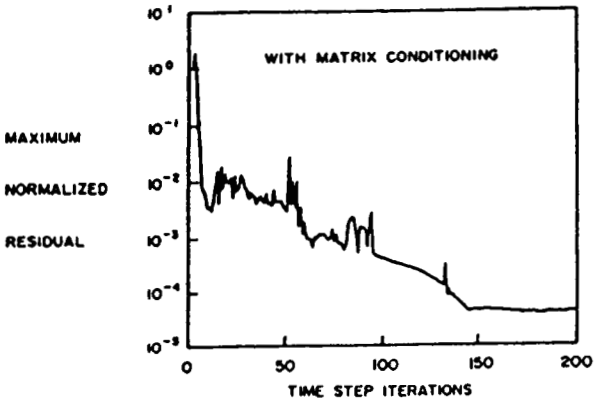

Fig. 6 Convergence Rate.

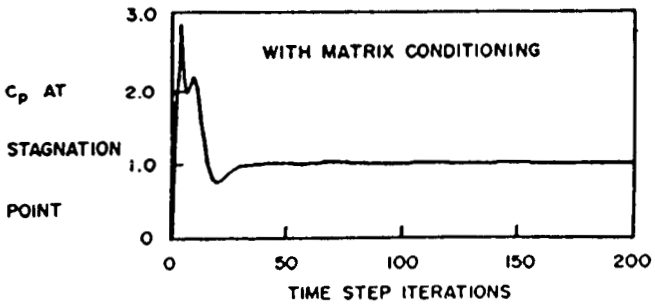

Fig. 7 Convergence of Pressure at Stagnation Point.

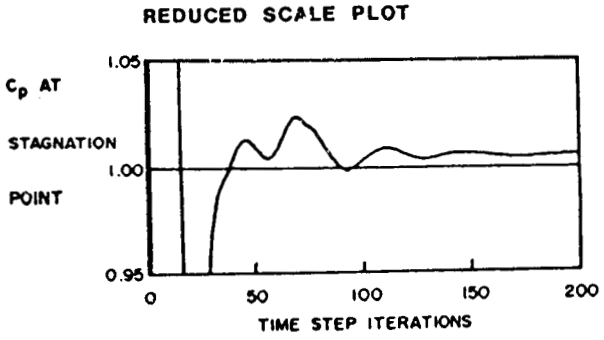

Fig. 8 Convergence of Pressure at Stagnation Point.

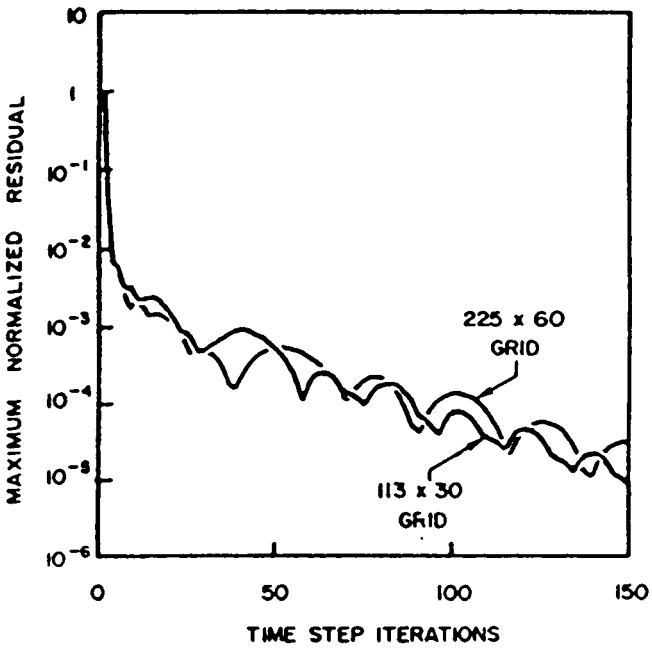

Fig. 9 Convergence Behavior, C3X Laminar 2-D Cascade.

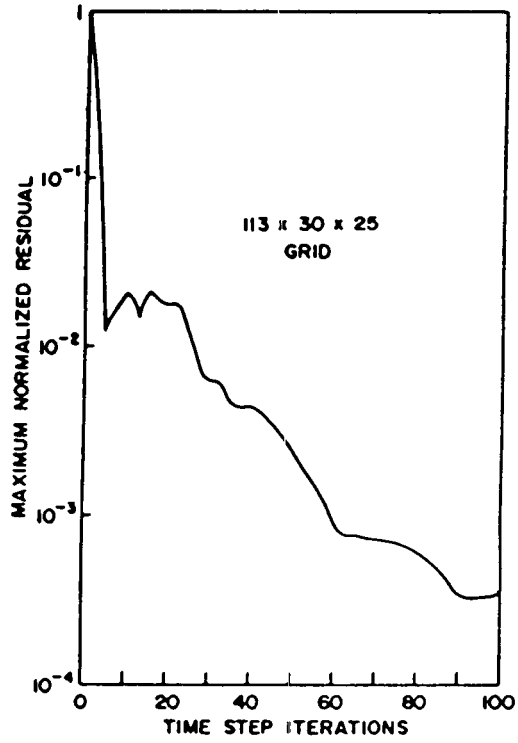

Fig. 10 Convergence Behavior, C3X Laminar 3-D Cascade.

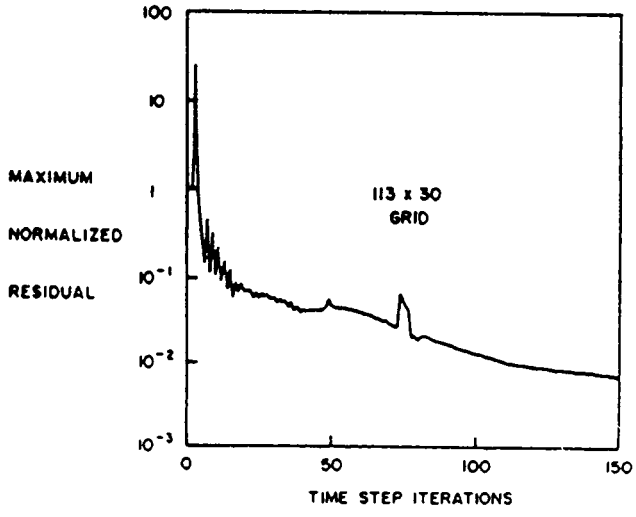

Fig. 11 Turbulent C3X Cascade.

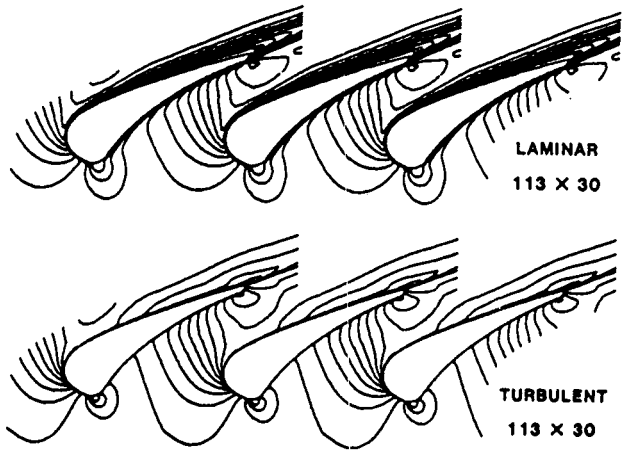

Fig. 12 C3X Cascade Mach Number Contours.

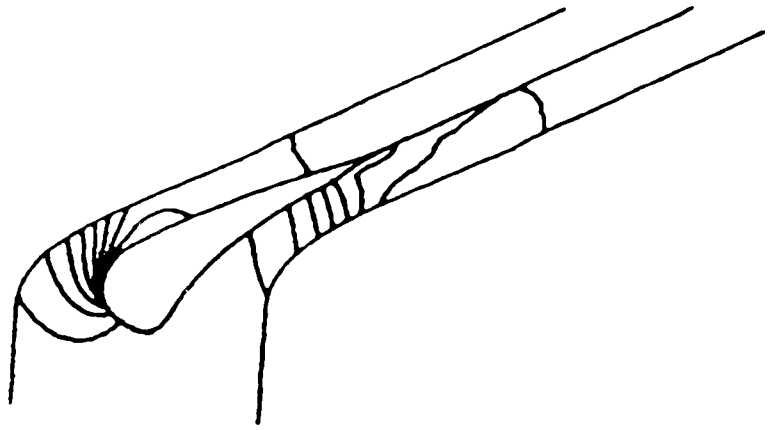

Fig. 13 Pressure Contours, C3X Cascade, Turbulent Flow, k-ε Model.

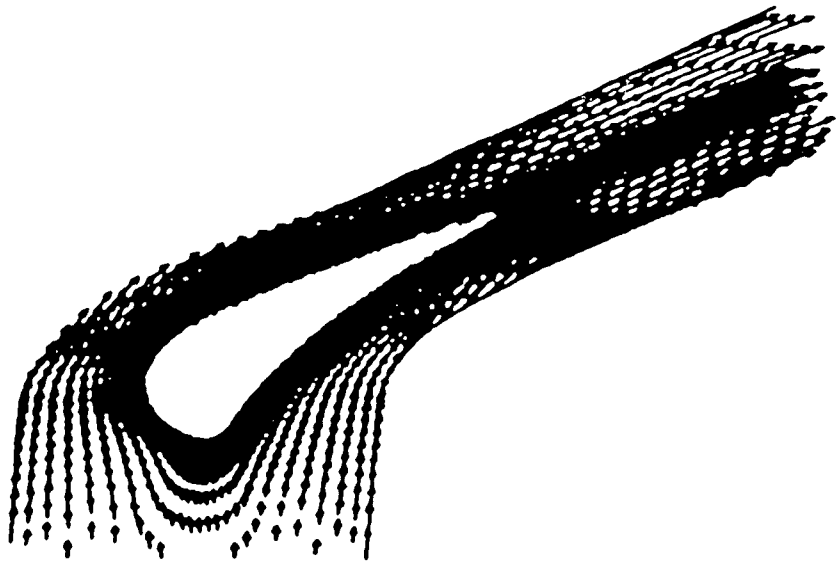

Fig. 14 Velocity Vectors, C3X Cascade, Turbulent Flow, k- ε Model.

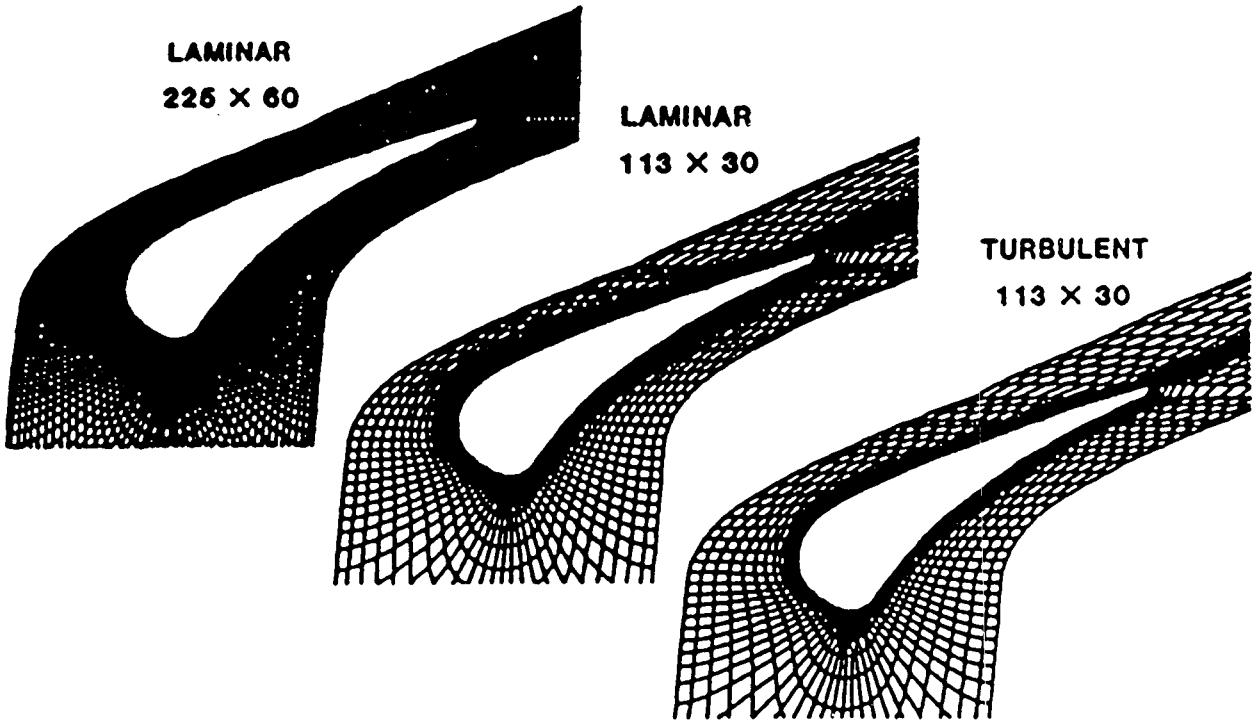

Fig. 15 C3X Grid for Three-Dimensional Calculation.

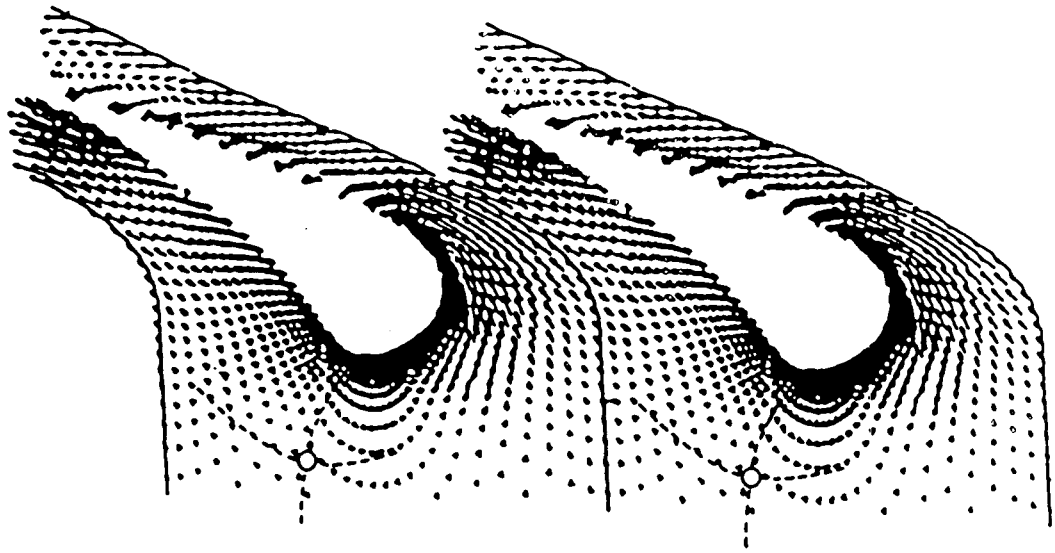

Fig. 16 C3X Three-Dimensional Calculation, Velocity Vectors in Plane Adjacent to Endwall.

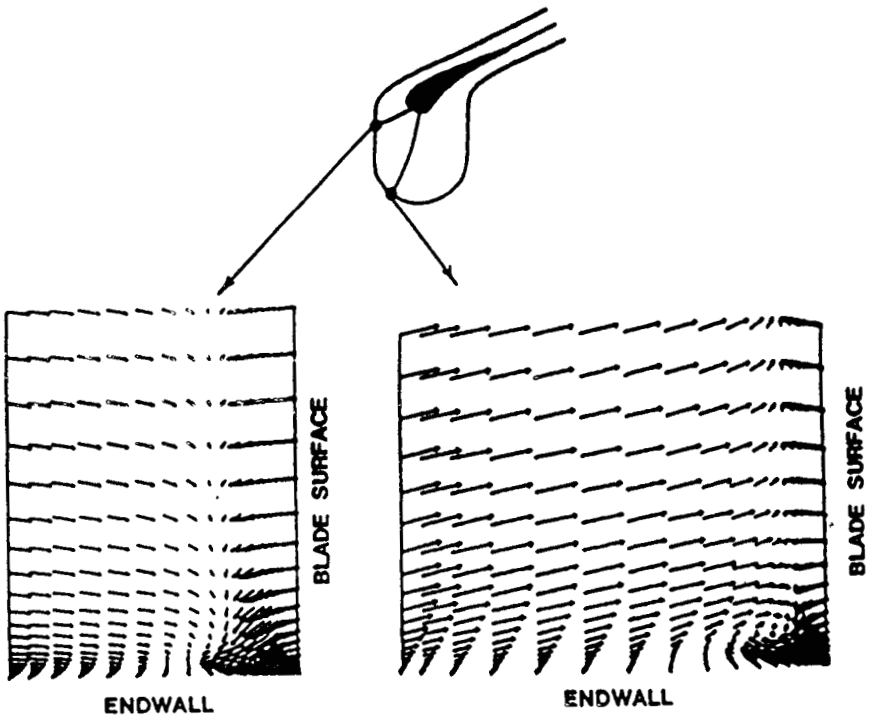

Fig. 17 C3x Three-Dimensional Calculation, Stagnation Region.